Detection of Fast-Changing Intra-seasonal Vegetation Dynamics of Drylands Using Solar-Induced Chlorophyll Fluorescence (SIF)

Jiaming Wen[1,2†*], Giulia Tagliabue[3†], Micol Rossini[3], Francesco Pietro Fava[4], Cinzia Panigada[3], Lutz Merbold[5], Sonja Leitner[6], Ying Sun[1*]

[1]School of Integrative Plant Science, Soil and Crop Sciences Section, Cornell University, Ithaca, NY, USA.
[2]Department of Global Ecology, Carnegie Institution for Science, Stanford, CA, USA.
[3]Remote Sensing of Environmental Dynamics Laboratory, Department of Environmental and Earth Sciences (DISAT), University of Milano - Bicocca, Milano, Italy.
[4]Department of Environmental Science and Policy, Università degli Studi di Milano, Milano, Italy.
[5]Integrative Agroecology Group, Research Division Agroecology and Environment, Agroscope, Reckenholzstr. 191, 8046 Zurich, Switzerland.
[6]International Livestock Research Institute, Mazingira Centre, P.O. Box 30709, 00100 Nairobi, Kenya.

[*]*Correspondence to*: Jiaming Wen (jwen@carnegiescience.edu), Ying Sun (ys776@cornell.edu)

†Jiaming Wen and Giulia Tagliabue contributed equally to this work.

This supplementary material includes Text S1 and Figures S1-S12. Text S1 describes the spatial and temporal matching criteria used in this study. Figures S1-S12 are supplementary figures to the main manuscript.

Text S1

In this supplementary section, we describe the spatial and temporal matching criteria used in this study. We employed slightly different spatial and temporal matching criteria for the analysis of SIF intercomparison (Section 2.5) and the analysis of intra-seasonal vegetation dynamics (Section 3). The principle is: for the SIF intercomparison against in situ SIF, we attempt to ensure the most consistency between in situ SIF and each satellite SIF dataset to be evaluated; for the intra-seasonal analysis, we attempted to ensure the consistency among all the datasets (including SIF and other ancillary variables) so that all the variables refer to the same spatial domains and time intervals.

Text S1.1 Spatial and temporal matching criteria for SIF intercomparison

Spatial matching: To compare with in situ SIF measurements, TROPOMI was aggregated to 0.15° pixel centered at the tower location. For the reconstructed SIF products, we extracted the value of the 0.05° pixel where tower resides to minimize the difference in spatial scales.

Temporal matching: For the paired comparison between in situ SIF and TROPOMI, we selected the quality-filtered in situ SIF observations (Section 2.2) collected within a time window of ±30 minutes with respect to the overpass time of each

TROPOMI observation. The selected measurements were averaged after applying the daily-correction factor based on the SZA, which was also applied to the TROPOMI SIF. The TROPOMI observations for which no in situ SIF observations were available in the ±30 minutes time window were discarded. In total, 64 data pairs were used for comparison.

For the paired comparison between in situ SIF and the reconstructed SIF products, we extracted the quality-filtered in-situ SIF within a ±30 minutes time window centered at the OCO-2 and TROPOMI nominal overpass time at the equator (i.e., 13:30 local solar time), applied the daily correction factor and then averaged the measurements across 4-, 8- or 16-day periods to match with the temporal resolution of the reconstructed products. In total, 67, 84, 40 and 55 data pairs were used for comparison for CSIF, GOSIF, SIF_oco2_005 and RTSIF, respectively.

Text S1.2 Spatial and temporal matching criteria for intra-seasonal analysis

We aggregated or resampled all the remote-sensing based datasets to the same 0.15° and 8-day resolutions. For the analysis of intra-seasonal dynamics at Kapiti (Section 3.1), we selected the quality-filtered in situ SIF observations (Section 2.2) collected within a time window of ±30 minutes with respect to the overpass time of TROPOMI and applied a daily-correction factor based on the SZA to convert them into daily values. The daily values were then aggregated to the same 8-day intervals.

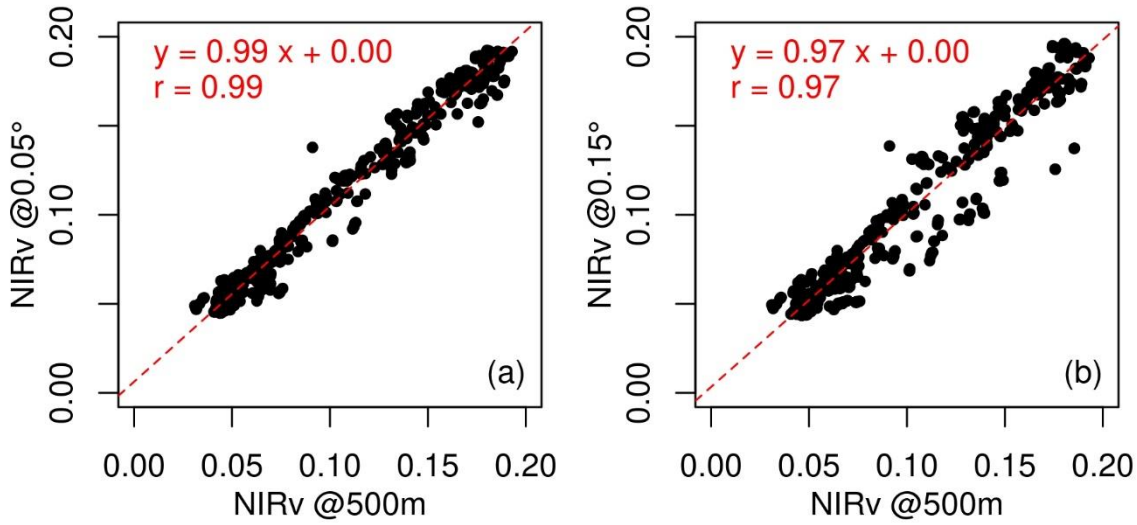

Figure S1: Comparison of daily MODIS NIRv at Kapiti extracted at (a) 500 m vs 0.05°, and (b) 500 m vs 0.15° pixels during 2019-2020. The temporal variations of different spatial scales are highly consistent.

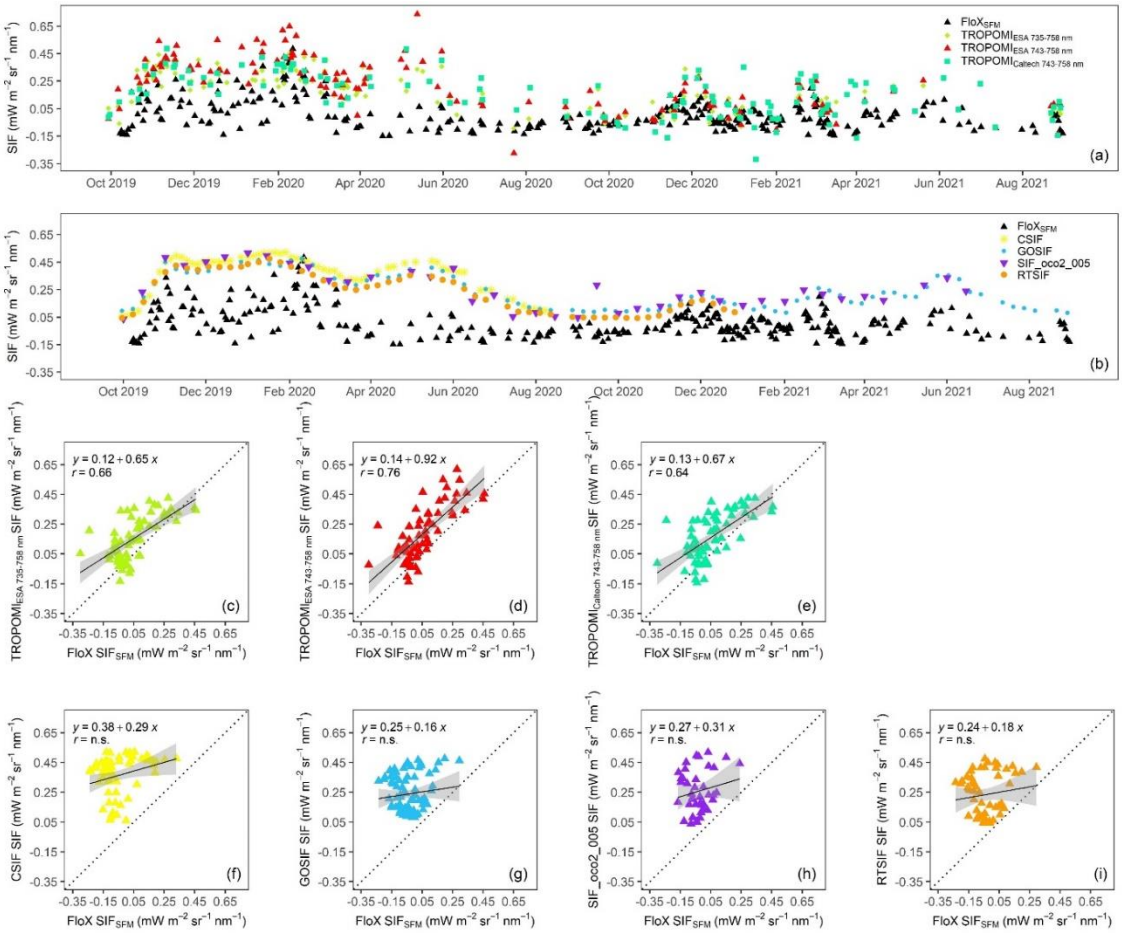

55 **Figure S2: Similar to Fig. 2, but with FloX SIF$_{SFM}$. Not significant correlations are indicated as n.s. (p>0.05).**

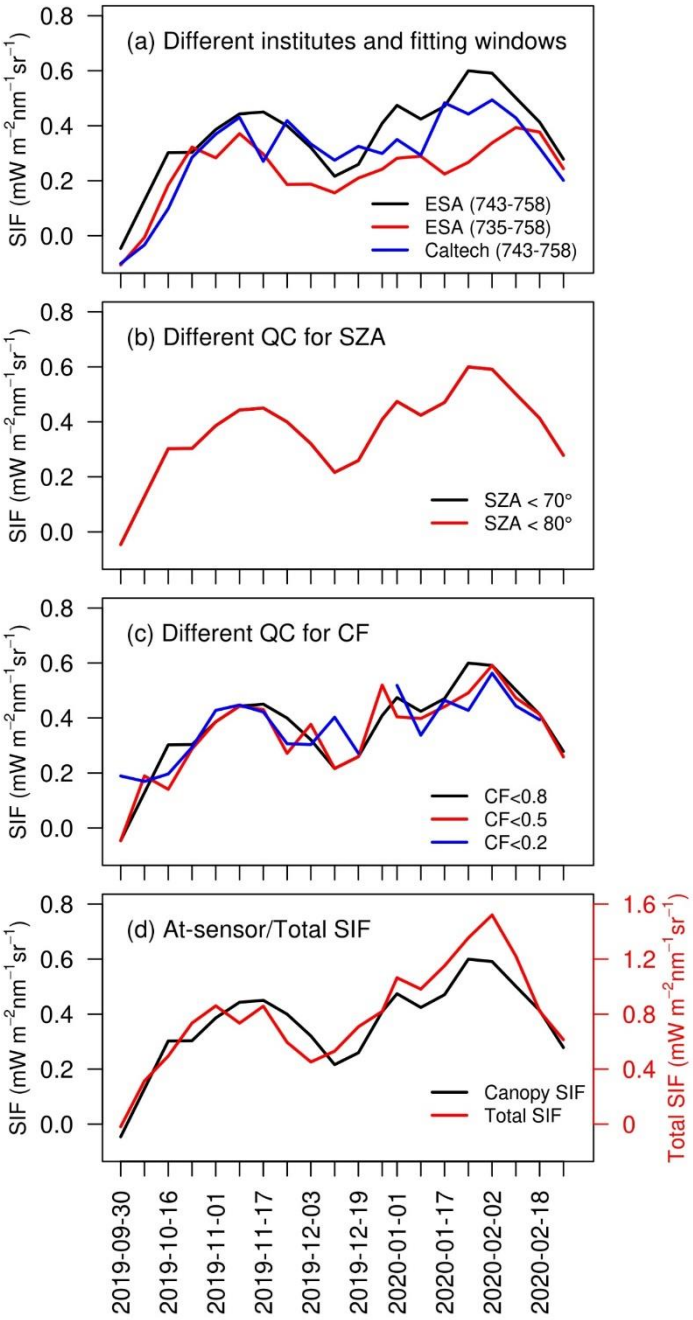

Figure S3: Sensitivity tests of TROPOMI SIF from October 2019 to February 2020, with (a) different fitting windows for SIF retrievals or data sources (ESA, Guanter et al. 2021; Caltech, Köhler et al., 2018); (b) different quality control (QC) filters for solar zenith angle (SZA) thresholds; (c) different QC filters for cloud fraction (CF) thresholds; and (d) whether SIF escape probability was accounted for, following Z. Zhang et al. (2020). Only one criterion varies for each panel relative to the baseline (used in the main analyses): ESA (743-758nm), SZA<70°, CF<0.8, at-sensor SIF. The black and red curves in (b) are completely overlapped with each other, indicating that the extracted TROPOMI time series is not sensitive to SZA thresholds for QC.

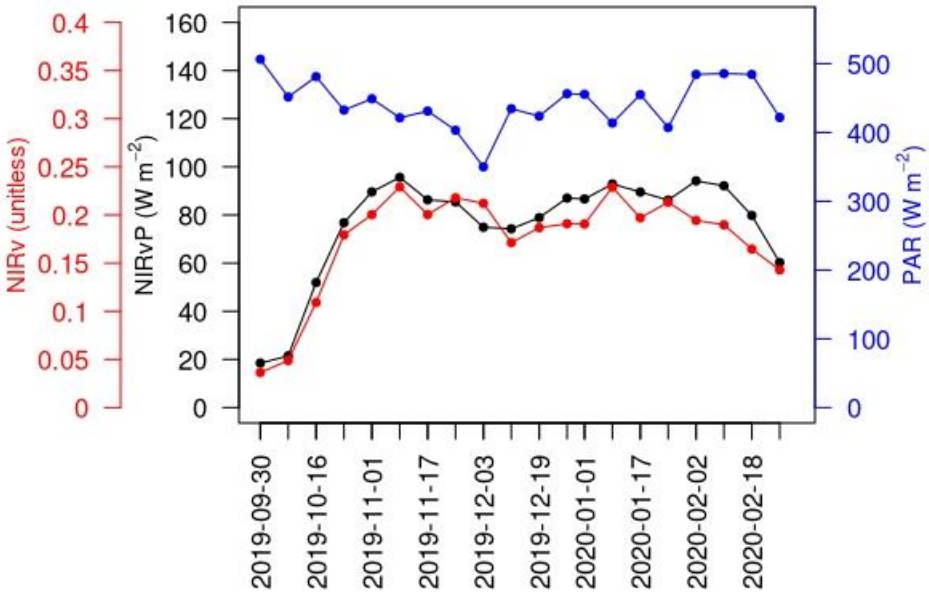

Figure S4: Time series of in situ incoming PAR (blue), NIRv (red) and NIRvP (= NIRv × PAR, black) from October 2019 to February 2020. The data was extracted at 13:30 ± 30 min local solar time and aggregated to 8-day intervals.

Figure S5: Phenocam images at Kapiti on (a) November 5th, 2019, (b) December 16th, 2019, and (c) February 8th, 2020. Some grasses reached the maturity stage in mid-December due to excessive water availability, while a second peak occurred in February 2020.

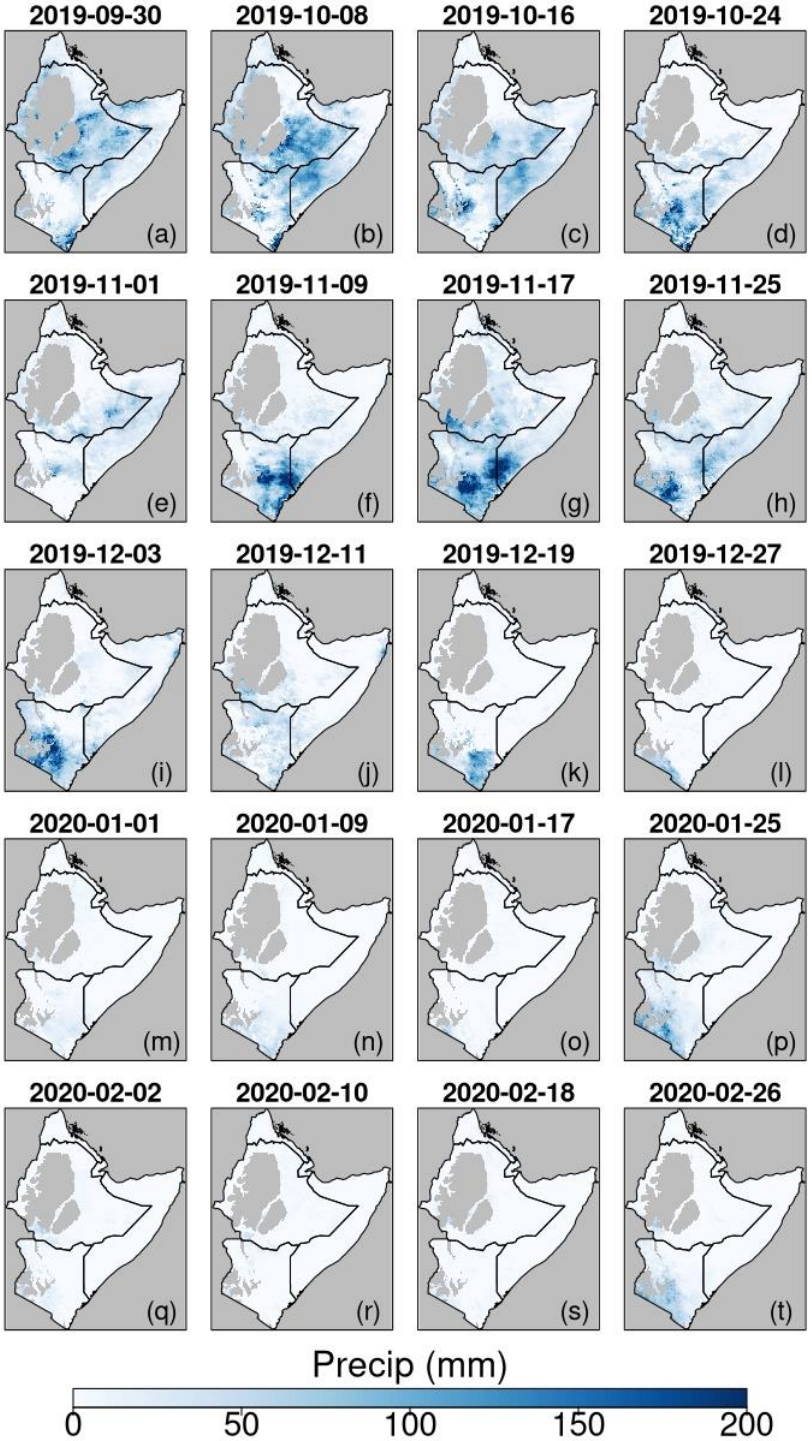

Figure S6: Spatial maps of precipitation in the HoA drylands during October 2019 and February 2020. The date labels represent the starting date of each 8-day period.

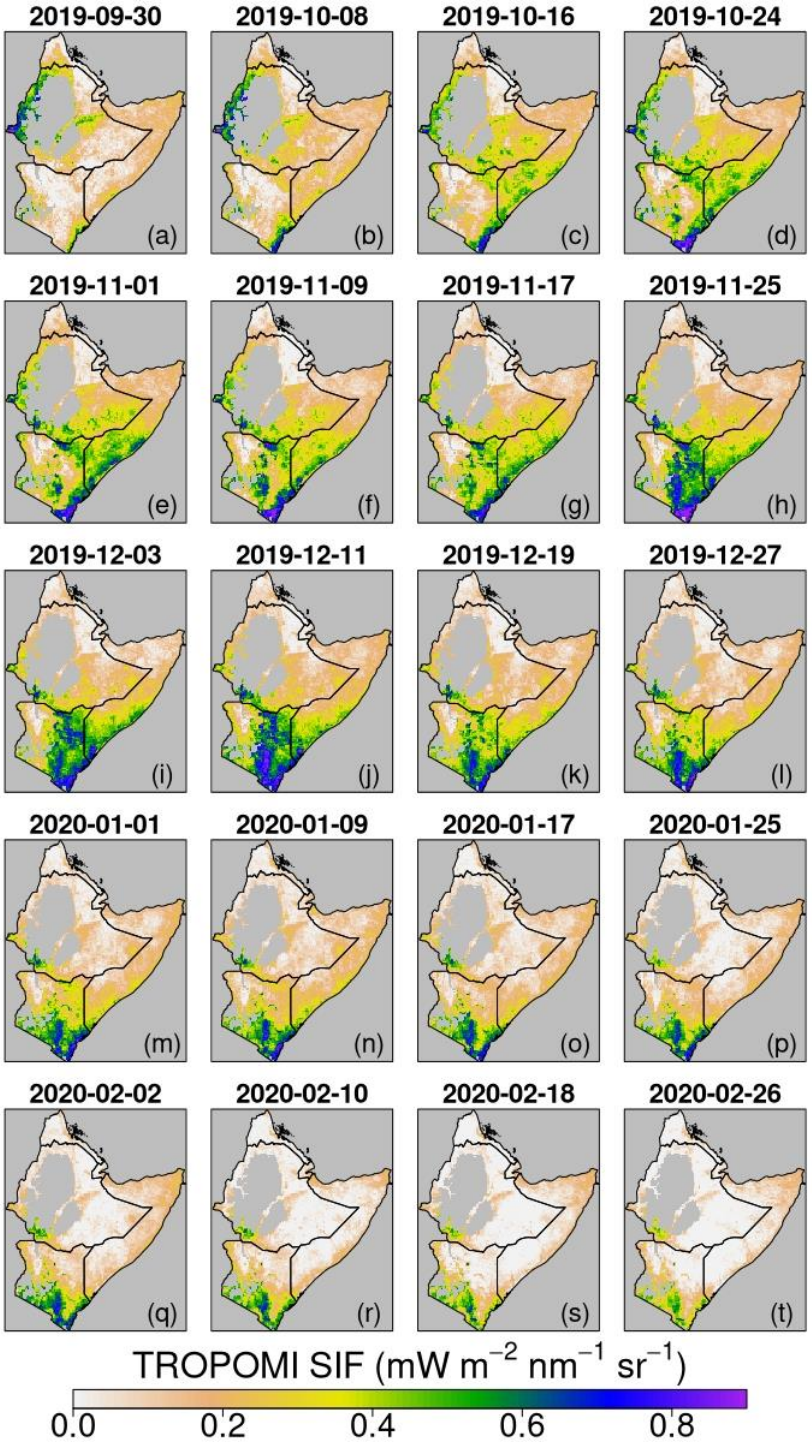

Figure S7. Spatial maps of TROPOMI SIF in the HoA drylands during October 2019 and February 2020. The date labels represent the starting date of each 8-day period.

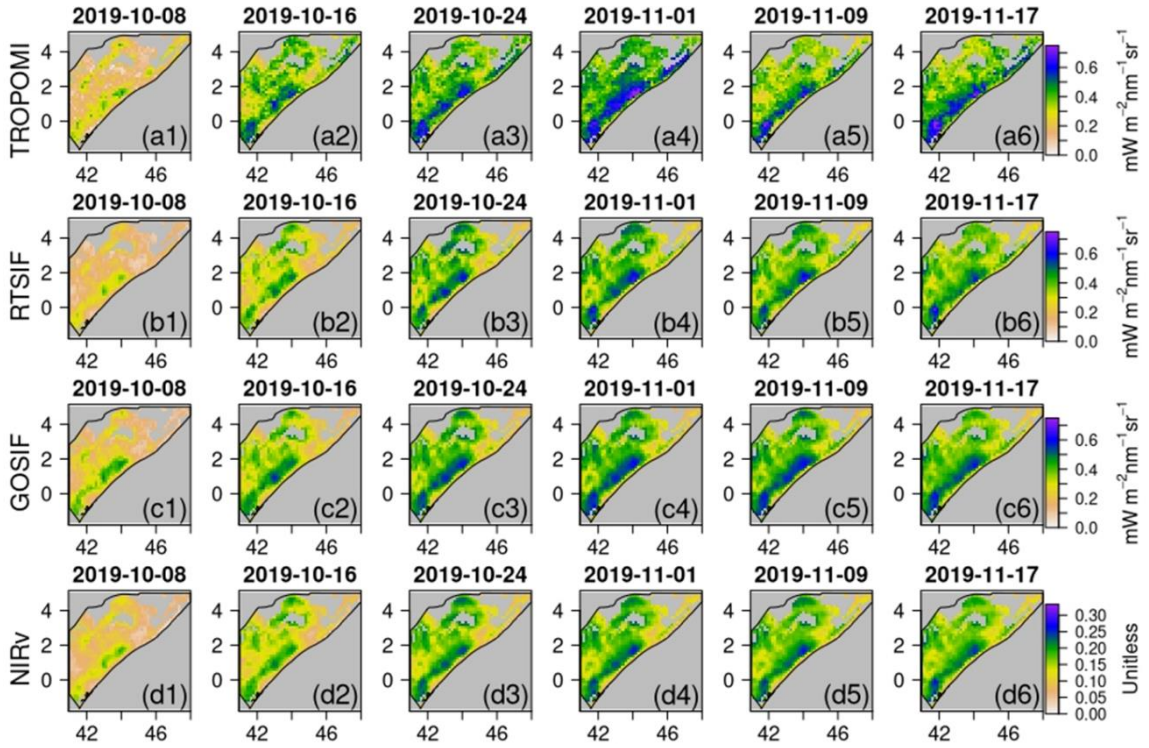

Figure S8. Intra-seasonal variations of (a) TROPOMI SIF, (b) RTSIF, (c) GOSIF, (d) MODIS NIRv in the grasslands of Region 2 during October 8th and November 17th, 2019. The date labels represent the starting date of each 8-day period.

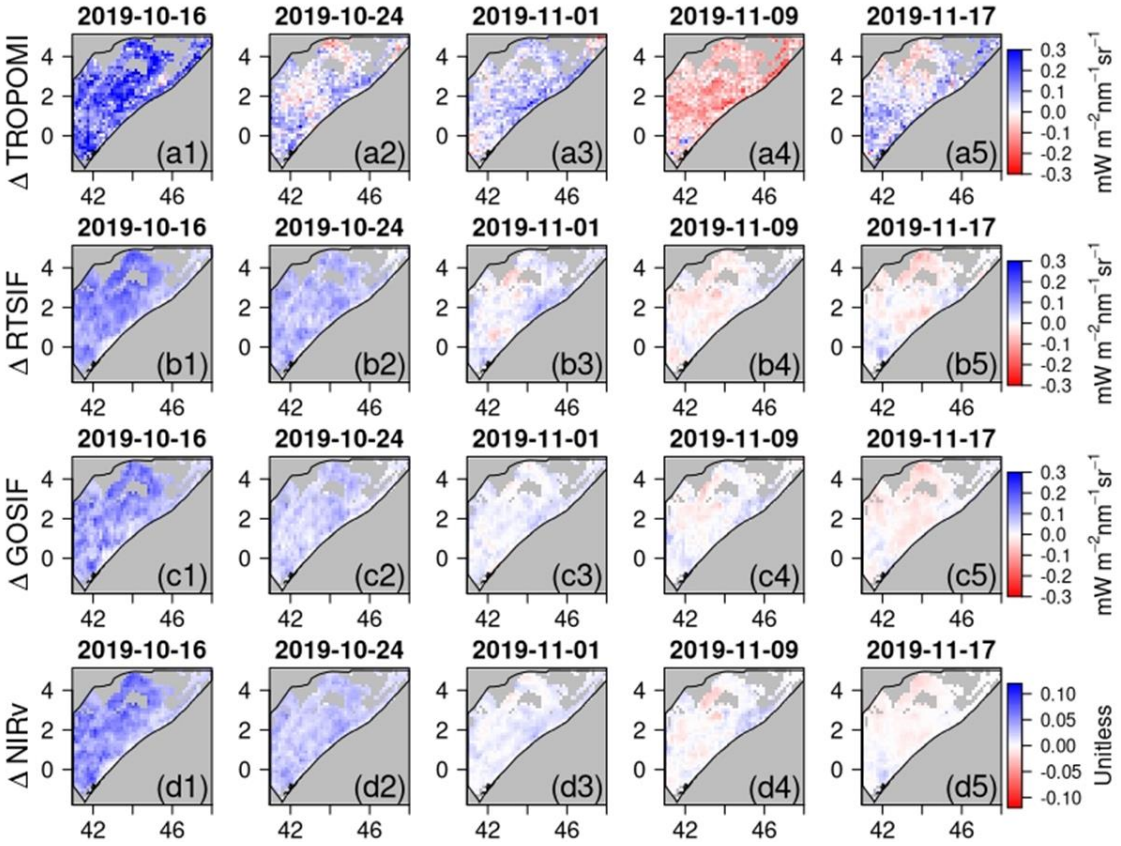

Figure S9: Temporal change rate of (a) TROPOMI SIF, (b) RTSIF, (c) GOSIF, (d) MODIS NIRv in the grasslands of Region 2 compared to the previous 8-day period during October 16th and November 17th, 2019. The date labels represent the starting date of each 8-day period.

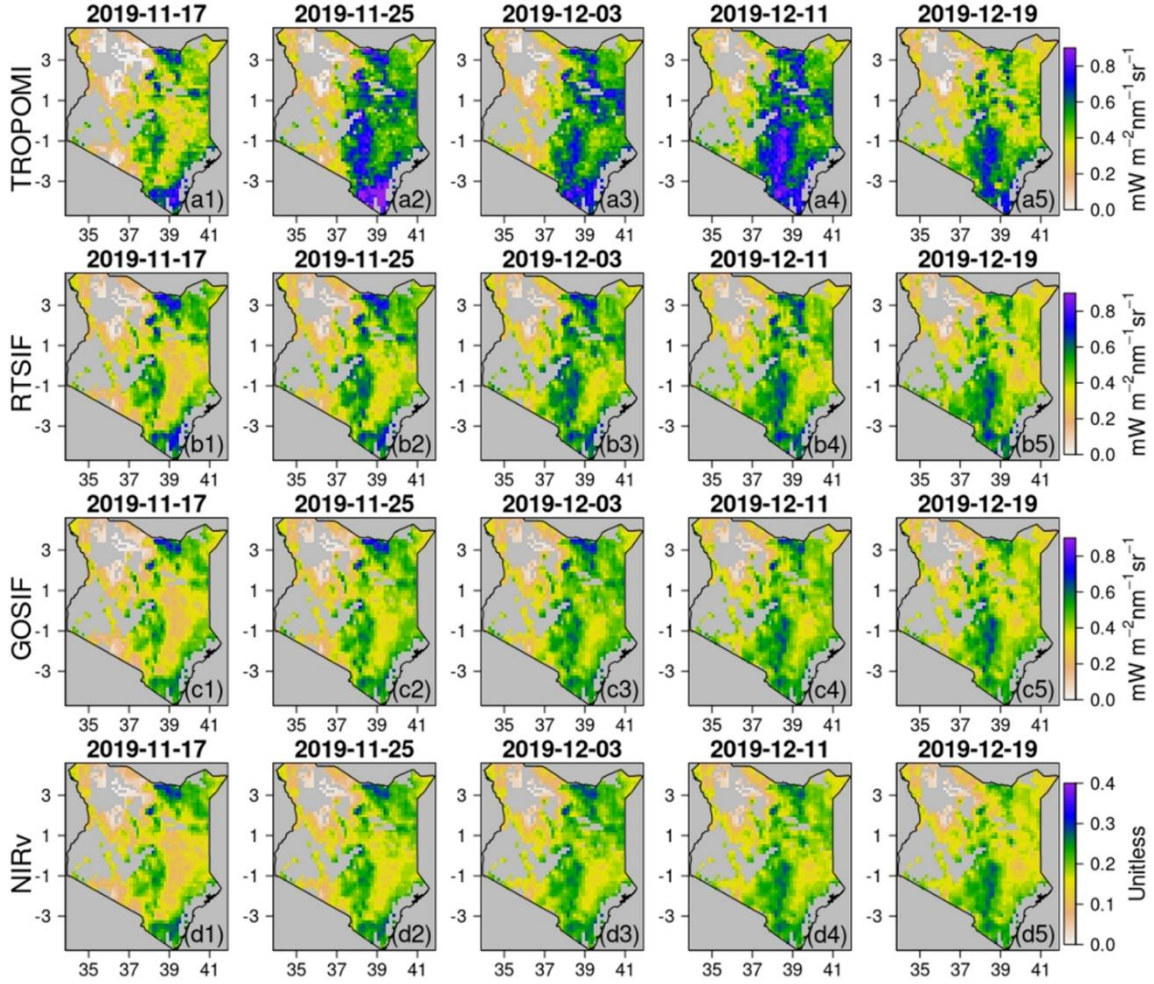

Figure S10: Intra-seasonal variations of (a) TROPOMI SIF, (b) RTSIF, (c) GOSIF, (d) MODIS NIRv in the grasslands of Region 3 during November 17th and December 27th, 2019. The date labels represent the starting date of each 8-day period.

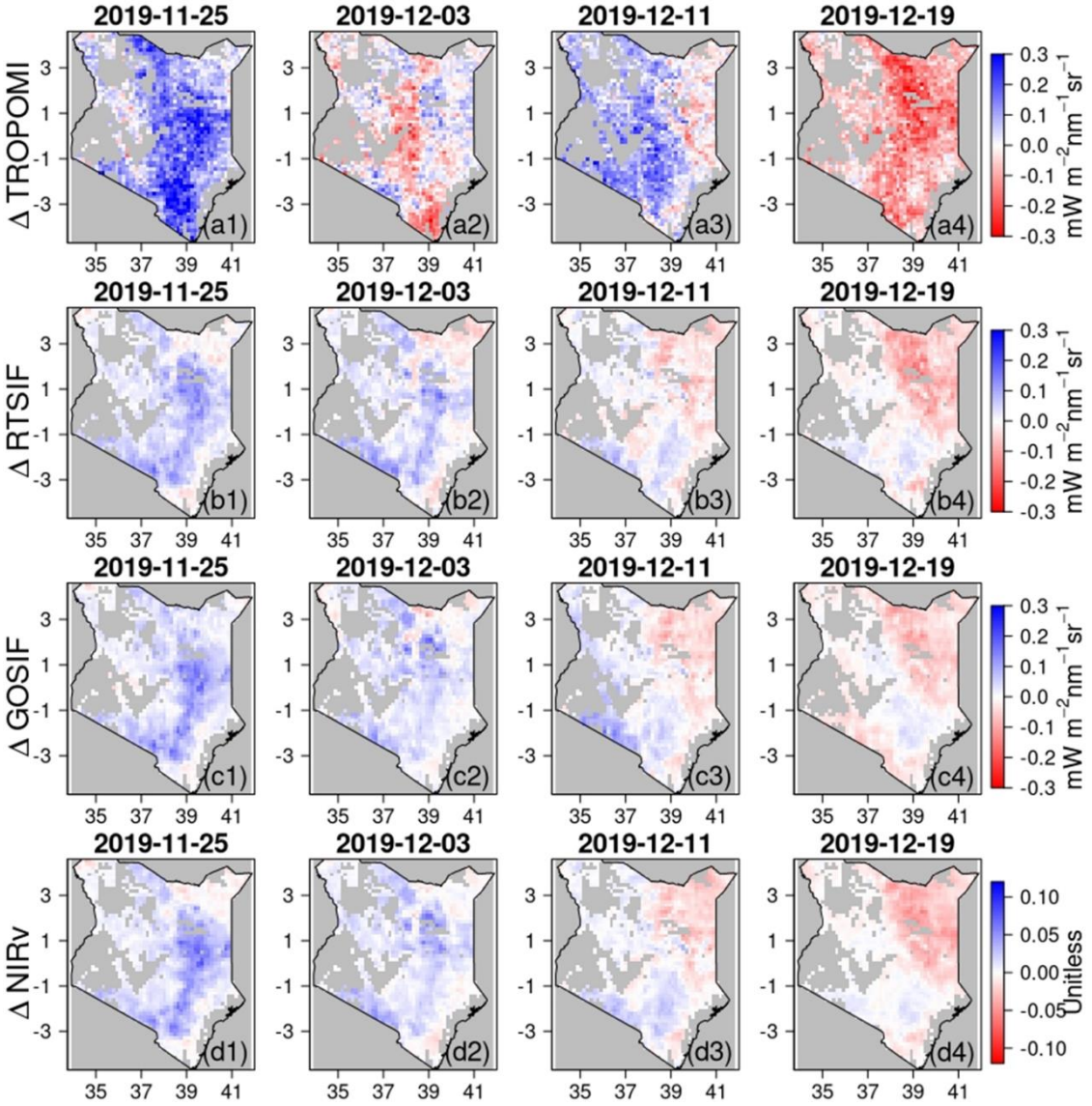

Figure S11: Temporal change rate of (a) TROPOMI SIF, (b) RTSIF, (c) GOSIF, (d) MODIS NIRv in the grasslands of Region 3 compared to the previous 8-day period during November 25 and December 27, 2019. The date labels represent the starting date of each 8-day period.

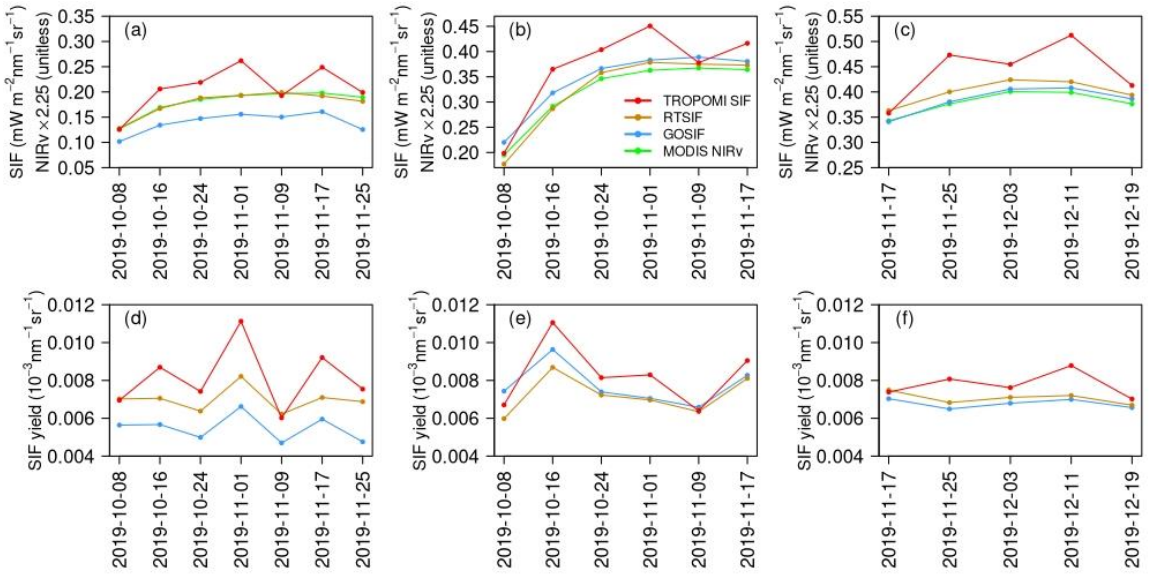

105 **Figure S12: Intra-seasonal variations of (a) – (c) SIF or NIRv and (d) – (f) SIF yield for the three sub-domains during the selected time windows (Fig. 4). The x axis labels represent the starting date of each 8-day interval.**